Cardiovascular Toxicology
https://doi.org/10.1007/s12012-024-09915-9

Exosomes from Hypoxic Pretreatment ADSCs Ameliorate Cardiac Damage Post-MI via Activated circ-Stt3b/miR-15a-5p/GPX4 Signaling and Decreased Ferroptosis

Jili Liu[1] · Zhaolin Wang[2] · Anhua Lin[3] · Na Zhang[4]

Received: 17 December 2023 / Accepted: 20 August 2024

Abstract
Accumulation studies confirmed that oxidative stress caused by ischemia after myocardial infarction (MI) is an important cause of ventricular remodeling. Exosome secretion through hypoxic pretreatment adipose-derived mesenchymal stem cells (ADSCs) ameliorates myocardial damaging post-MI. However, if ADSCs exosome can improve the microenvironment and ameliorate cardiac damage post-MI still unknown. Next-generation sequencing (NGS) was used to study abnormally expressed circRNAs in hypoxic pretreatment ADSC exosomes (HExos) and untreated ADSC exosomes (Exos). Bioinformatics and luciferase reporting were used to elucidate interaction correlation related to circRNA, mRNA, and miRNA. HL-1 cells were used to analyze the reactive oxygen species (ROS) and apoptosis under hypoxic conditions using immunofluorescence and flow cytometry. An MI mouse model was constructed and the therapeutic effect of Exos was determined using immunohistochemistry, immunofluorescence, and ELISA. The results showed that HExos had a more pronounced treatment effect than ADSC Exos on cardiac damage amelioration after MI. NGS showed that circ-Stt3b plays a role in HExo-mediated cardiac damage repair after MI. Overexpression of circ-Stt3b decreased apoptosis, ROS level, and inflammatory factor expression in HL-1 cells under hypoxic conditions. Bioinformatics and luciferase reporting data validated miR-15a-5p and GPX4 as downstream circ-Stt3b targets. GPX4 downregulation or miR-15a-5p overexpression reversed protective effect regarding circ-Stt3b upon HL-1 cells after exposure to a hypoxic microenvironment. Overexpression of circ-Stt3b increased the treatment effect of ASDSC Exos on cardiac damage amelioration after MI. Taken together, the study results demonstrated that Exos from hypoxic pretreatment ADSCs ameliorate cardiac damage post-MI through circ-Stt3b/miR-15a-5p/GPX4 signaling activation and decreased ferroptosis.

Keywords Adipose-derived mesenchymal stem cells · Myocardial infarction · Exosomes · Circ-Stt3b · Ferroptosis

Introduction

Myocardial ischemia (MI) is among the main mortality causes worldwide, which often causes sudden death [1]. An increased number of studies has found that reactive oxygen

Handling Editor: Yajing Wang.

Jili Liu and Zhaolin Wang have contributed equally to this manuscript.

✉ Anhua Lin
linanhua999@163.com

✉ Na Zhang
zhangna2903@126.com

[1] Department of Geriatrics, The First Hospital, Shanxi Medical University, Taiyuan 030001, Shanxi, China

[2] Department of Traditional Chinese Medicine, The Second Hospital, Shanxi Medical University, Taiyuan 030001, Shanxi, China

[3] Department of Endocrinology, Jiangxi Provincial People's Hospital, The First Affiliated Hospital of Nanchang Medical College, No. 152, Aiguo Road, Donghu District, Nanchang 330006, Jiangxi, China

[4] Department of Hematology, Shanxi Hospital of Traditional Chinese Medicine, No. 46, Bingzhou West Street, Taiyuan 030012, Shanxi, China

Published online: 27 August 2024

species (ROS) induced by MI have an important function in myocardial damage. One recent investigation has further demonstrated that ferroptosis regulates chemotherapy fate and MI/R-caused cardiomyopathy [2]. Ferroptosis has now been appreciated as a type of oxidative cell death with distinct properties and functions, and is prominently characterized by the accumulation of lethal lipid ROS which is initiated by the peroxidation of phospholipids having polyunsaturated fatty acid (PUFA) chains [3]. Ferroptosis results in a novel class of programmed cell death that depicted via iron-dependent aggregation of lipid peroxides in toxic ranges [4, 5]. Therefore, uncovering the specific ferroptosis mechanism may provide an approach for reducing myocardial injury after MI [6, 7].

Accumulated studies confirm that hypoxia-elicited mesenchymal stem cells possess cardiac repair effects after myocardial infarction (MI) [8]. Adipose-derived stem cell (ADSC) transplantation can attenuate ischemic disease-induced damage by promoting cell repair along with regeneration abilities [9]. Seeking to avoid the safety risks of stem cell transplantation, former investigations found that exosomes from ADSCs have a therapeutic effect [10]. Former investigations showcased that exosomes from ADSCs ameliorate cardiac damaging post-MI via S1P/S1PR1/SK1 signaling activation and macrophage M2 polarization promotion [11]. Exosomes from ADSCs prevent oxidative stress-induced cardiomyocyte apoptosis [12].

Exosomes are microvesicles 40–150 nm in diameter that carry ncRNAs [13, 14]. circular RNAs (circRNAs) belong to a class of closed ncRNA molecules that produced via back splicing of exons in eukaryote precursor mRNAs [15]. Previous investigations have found that circFndc3b modulates cardiac repair post-MI through the FUS/VEGF-A axis [16]. circRNA 010567 enhances MI rats through suppressing TGF-beta1 [17]. Nevertheless therapeutic effect of ADSC exosomes on MI related to circRNA delivery remains unclear. Therefore, the present investigation aimed to validate specific ADSC-derived exosomal circRNA effects on MI-induced ferroptosis and myocardial damage.

In the present study, we propose that Exos from hypoxic pretreatment ADSCs ameliorate cardiac damage post-MI through circ-Stt3b/miR-15a-5p/GPX4 signaling activation and decreased ferroptosis. Our findings provide new insights into the pathogenic mechanisms of myocardial ischemia injury and identify potential therapeutic targets for MI.

Materials and Methods

ADSC Isolation

Adipose tissue were obtained from normal mice and subsequently washed with phosphate-buffered saline (PBS) and mechanically chopped prior to digestion with 0.2% collagenase I (Sigma–Aldrich, Milwaukee, WI, USA) for 1 h at 37 °C with intermittent shaking. Tissues were digested in Dulbecco's Modified Eagle's Medium (DMEM; Sigma-Aldrich) with 15% fetal bovine serum (FBS), which were centrifuged at 1000×*g* for 10 min to eliminate mature adipocytes. Cell pellet were resuspended in DMEM supplemented with 15% FBS, 100 µg/mL streptomycin, 100 U/mL penicillin that incubated at 37 °C with 5% CO_2. After achieving 80–90% confluency, we treated ADSCs utilizing 0.02% EDTA/0.25% trypsin (Sigma–Aldrich) for 5 min at room temperature as well as replated afterwards. Phycoerythrin was used in phenotypic analysis. The CD29, CD90, CD44, CD105, CD34, and von Willebrand factor (vWF) expressions were also studied. ADSCs were cultured under normoxic conditions in 5% CO_2 and 95% air (20% O_2). For hypoxic pretreatment, ADSCs were cultured in hypoxic conditions of 5% CO_2, 93% N_2 and 2% O_2 [18].

ADSC Multilineage Differentiation

To characterize ADSCs' ability for multilineage differentiation, we cultured 3rd passage mice ADSCs under differentiation conditions. For adipocyte differentiation, ADSCs were cultured in adipogenic differentiation medium followed by Oil Red O staining and detection of adipocyte differentiation after 2 weeks. For osteoblast differentiation, ADSCs were cultured in osteogenic differentiation medium that stained with alizarin red to detect osteogenesis after 3 weeks.

ADSC-EXO Isolation and Identification

The ADSCs were cultivated in EGM-2MV medium with no FBS, which we supplemented with 1× serum replacement solution (PeproTech, New Jersey, USA) for 2 more days and then rinsed with PBS after achieving 80–90% confluency. Conditioned medium from ADSCs was first centrifuged at 300×*g* for 10 min, followed by centrifugation at 2000×*g* for 10 min to eliminate cellular debris and apoptotic cells. Finally, supernatant samples, after centrifugation at 12,000×*g* for 0.5 h, were filtered with 0.22-µm filters (Millipore, Billerica, MA, USA). We added a total of 15 mL supernatant to 100 kDa Amicon Ultra-15 Centrifugal Filter Unit (Millipore) which were centrifuged at 4000×*g*, to obtain a 1-mL sample. Ultrafiltration liquid was cleaned two times using PBS, followed by ultracentrifugation at 4000×*g* to again obtain 1-mL samples. The experiments were performed at 4 °C. We defined protein exosome content applying Pierce BCA Protein Assay Kit (Thermo Fisher Scientific, MA, USA) and stored ADSC EXOs at − 80 °C or utilized for downstream experiments. Western blotting along with transmission electron microscopy were applied to characterize exosomes.

Myocardial Cell Culture and Hypoxia Injury Model Preparation

We obtained HL-1 cell line from Shanghai Cell Bank, Chinese Academy of Medical Sciences. We cultured cells in 25-cm^2 cell culture flasks (Corning, USA) in DMEM (Invitrogen, Waltham, MA, USA) with 10% FBS (Invitrogen) at 37 °C with 5% CO_2 and 95% air for the following experiments. For hypoxic environment, we stored cells at 37 °C with 93% N_2, 5% CO_2, and 2% O_2 for 1 day.

Strand-Specific NGS Library

Total RNA samples from ADSC exosomes and hypoxic pretreatment ADSC exosomes were obtained using the TRIzol reagent (Invitrogen, Carlsbad, CA, USA). About 3 μg total RNA from each sample were processed using VAHTS Total RNA-seq (H/M/R) Library Prep kits from Illumina (Vazyme Biotech Co., Ltd, Nanjing, China) to eliminate ribosomal RNA as well as retain mRNAs and ncRNAs. RNA samples were treated with 40 U of RNase R (Epicenter) for 3 h at 37 °C followed by TRIzol purification. The RNA-seq lib were generated using KAPA Stranded RNA-Seq Library Prep kits (Roche, Basel, Switzerland), which were applied for NGS (Illumina HiSeq 4000 at Aksomics, Inc., Shanghai, China).

Quantitative Reverse Transcription-PCR (qRT-PCR)

RNA were extraction following TRIzol protocols for cDNA synthesis utilizing TaqMan Reverse Transcription Reagents kit (Applied Biosystems, Foster City, CA, USA). The primers were: circ-Stt3b, 5′-CAGCAAGAGAGTC-3′ and 5′-CAAGATGATGTGTTG-3′; miR-15a-5p, 5′-TAGCAGCACATAATGGTTTGTG-3′ and 5′-CTCAACTGGTGTCGTGGA-3′; GPX4, 5′-AGTACAGGGGTTTCGTGTGC-3′ and 5′-CATGCAGATCGACTAGCTGAG-3′; U6, 5′-CTCGCTTCGGCAGCACA-3′ and 5′-ACGCTTCACGAATTTGCGTGTC-3′; and GAPDH, 5′-GCACCGTCAAGCTGAGAAC-3′ and 5′-TGGTGAAGACGCCAGTGGA-3′. ABI 7900 thermocycler (Applied Biosystems) was applied to make qRT-PCR. Each cDNA sample were tested in triplicate. Relative mRNA expression quantifications were performed employing $2^{-\Delta\Delta Ct}$ method. The result were normalized data to *U6* and *GAPDH*.

ELISA

TNF-α, IL-1β, and IL-6 inflammatory cytokine levels in conditioned HL-1 cell medium and animal circulation were defined utilizing ELISA kits following manufacturer protocols. ELISA kits were purchased from Multi Sciences Biotech (Hangzhou, China).

MI Model

Acute MI was induced in mice. Female rats aged 6 weeks were anesthetized with pentobarbital at concentration of 30 mg/kg body weight via intraperitoneal injection. Thoracotomy was performed post-anesthesia to expose the left ventricle. Left anterior descending artery was ligated between left atrium and pulmonary artery outflow tract. Mice were randomly divided into three subgroups after MI surgery as follows: mice with intravenous tail vein injections of 500 μL of PBS (PBS group), 2×10^{10} particles of ADSC-derived exosomes, and hypoxic pretreatment ADSCs or circ-Stt3b overexpression ADSCs suspended in 500 μL of PBS. The mice were anesthetized and murdered, the heart were isolated for immunohistochemical detection on day 28 post-MI.

Histological Examination

To assess apoptosis, myocardial tissues or cardiomyocytes were labeled and fixed using a terminal deoxynucleotidyl transferase-mediated dUTP-biotin nick end labeling (TUNEL) and In Situ Cell Death Detection Kit (Roche Diagnostics) to identify apoptotic cell nuclei. To characterize myocardial tissue damage, myocardial tissue samples were stained using Masson. We examined sections utilizing Axiophot light microscope (Zeiss, Oberkochen, Germany) and photographed with digital camera.

ROS Activity

Intracellular ROS generation was assessed using the dichloro-dihydro-luorescein diacetate (DCFH-DA) assay (Beyotime, China). We incubated HL-1 cells or myocardial tissue samples with DCFH-DA for 30 min at 37 °C in the dark. Fluorescence were measured at 525 nm emission and 488 nm excitation utilizing fluorescence microplate reader (PerkinElmer, USA).

Flow Cytometry

Cytometry were employed to detect HL-1 cell apoptosis rate. We differentiated apoptotic cells from necrotic or viable cells via a combination of propidium iodide (PI) staining and annexin V (AV)-FITC. Technician washed cells twice to achieve 1×10^6 cells/mL concentration with cold D-Hanks buffer. Technician added 10 μL PI and equal volume of AV-FITC to 100-μL cell suspension as well as incubated for 15 min at room temperature in dark. Lastly, 400 μL binding buffer were added to every sample without

washing, which were then analyzed utilizing flow cytometry. Each experiment was repeated three times.

Luciferase Reporter Assay

To determine if miR-15a-5p regulated GPX4 expression directly and to study regulation between circ-Stt3b and miR-15a-5p, the 3′-untranslated region (UTR) sequences for circ-Stt3b and GPX4 were inserted into the downstream Renilla luciferase open reading frame in pGL3-CMV vector (Promega, Madison, WI, USA). We transfected HEK293T cells utilizing pGL3-basic constructs via scrambled control or miR-15a-5p mimic from Lipofectamine 2000 (Invitrogen). After 2 days, we harvested cells to measure their luciferase activities. Data were expressed by the rate for Renilla luciferase over firefly luciferase activity. We carried experiments out at Yingbai Corporation (Shanghai, China).

Statistics Analyses

We expressed data by mean ± SD. We determined statistical significance applying variance analysis and Tukey–Kramer multiple comparison test along with Student's *t*-test. $P < 0.05$ was regarded as statistical significance.

Results

ADSC-Exosome Characterization

The present study isolated ADSCs with classical cobblestone-like morphology (Fig. 1A). Immunofluorescence staining revealed positive cell surface expression for mesenchymal cell markers CD29, CD105, CD90, and CD44, and negative expression for endothelial markers CD34 and vWF (Fig. 1B–G). Oil red O and alizarin red staining results validated osteoblast and adipocyte differentiation (Fig. 1H, I). The exosomes were then isolated from ADSCs. ADSC exosomes were with sphere- or cup-shaped morphologies on transmission electron micrographs (Fig. 1J), which were similar to those in previous reports [19]. Exosome marker protein expression of CD63 and CD81 was obtained using Western blotting (Fig. 1K). Outcomes confirmed that the nanoparticles were exosomes.

Hypoxic Pretreatment ADSC Exosomes (HExos) have Greater Treatment Effect than ADSC Exosomes (Exos) on Ameliorating Cardiac Damage Post-MI

Exosomal protective effects on MI were assessed using histological analysis. Masson's trichrome staining was utilized to calculate infarcted tissue size after 4 weeks of treatment. The fibrotic area was stained blue in the imaging results, showing that HExos have a greater therapeutic effect by decreasing the MI-induced myocardial damage compared to Exos (Fig. 2A, B). Immunofluorescence ROS detection results showed that HExos have a greater therapeutic effect by decreasing the MI-induced myocardial ROS level in the infarction area (Fig. 2C, D). TUNEL staining showed that HExos have a greater therapeutic effect by decreasing MI-induced myocardial apoptosis (Fig. 2E, F). ELISA demonstrated that HExos have greater therapeutic effects than Exos by reducing MI-induced inflammatory cytokines TNF-α, IL-6 and IL-1β expression in serum (Fig. 2G–I).

Circ-Stt3b Functions in HExo-Mediated Cardiac Damage Repairing After MI

The accumulated evidences showcase that circRNAs function importantly in ADSC exosome-mediated disease treatment [20]. In order to reveal whether the high level of the therapeutic HExo effect relates to circRNA delivery, NGS analysis was employed to identify circRNA expressions among ADSC Exos and HExos (Fig. 3A). RT-qPCR experiments showed the upregulated circRNA expression of mmu_circ_0001852, mmu_circ_0001090, mmu_circ_0001774, mmu_circ_0006764, mmu_circ_0001053, mmu_circ_0001732, mmu_circ_0000713, and mmu_circ_0000905. Results revealed that mmu_circ_0001852 expression incremented significantly in HExos comparing to Exos (Fig. 3B). qRT-PCR data showcased that mmu_circ_0001852 expression decremented in MI mouse serum (Fig. 3C). Then, the mmu_circ_0001852 overexpression vector was constructed and transfected into HL-1 cells. Data showcased that mmu_circ_0001852 expression increased significantly in the mmu_circ_0001852 overexpression group (Fig. 3D).

HL-1 cell apoptosis was evaluated using flow cytometry, and data showcased that hypoxic conditions enhanced HL-1 cell apoptosis. However, mmu_circ_0001852 upregulation decreased hypoxia-induced cell apoptosis (Fig. 3E, F). ELISA detection of inflammatory cytokine IL-1β, TNF-α and IL-6 expressions demonstrated that mmu_circ_0001852 upregulation decreased hypoxia-induced inflammatory cytokine expression (Fig. 3G–I). The mmu_circ_0001852 was generated by cyclizing four exons from the *Stt3b* gene at chr9:115175211-115189637. Stt3b is 14,426 bp in length, while the spliced mature circRNA is 563 bp in length, so we also named mmu_circ_0001852 as circ-Stt3b (Fig. 3J).

miR-15a-5p and GPX4 are circ-Stt3b Downstream Targets

Bioinformatics data discovered that circ-Stt3b may interact with miRNAs, such as miR-15a-5p. Luciferase reporter data verified that miR-15a-5p suppressed luciferase activity in

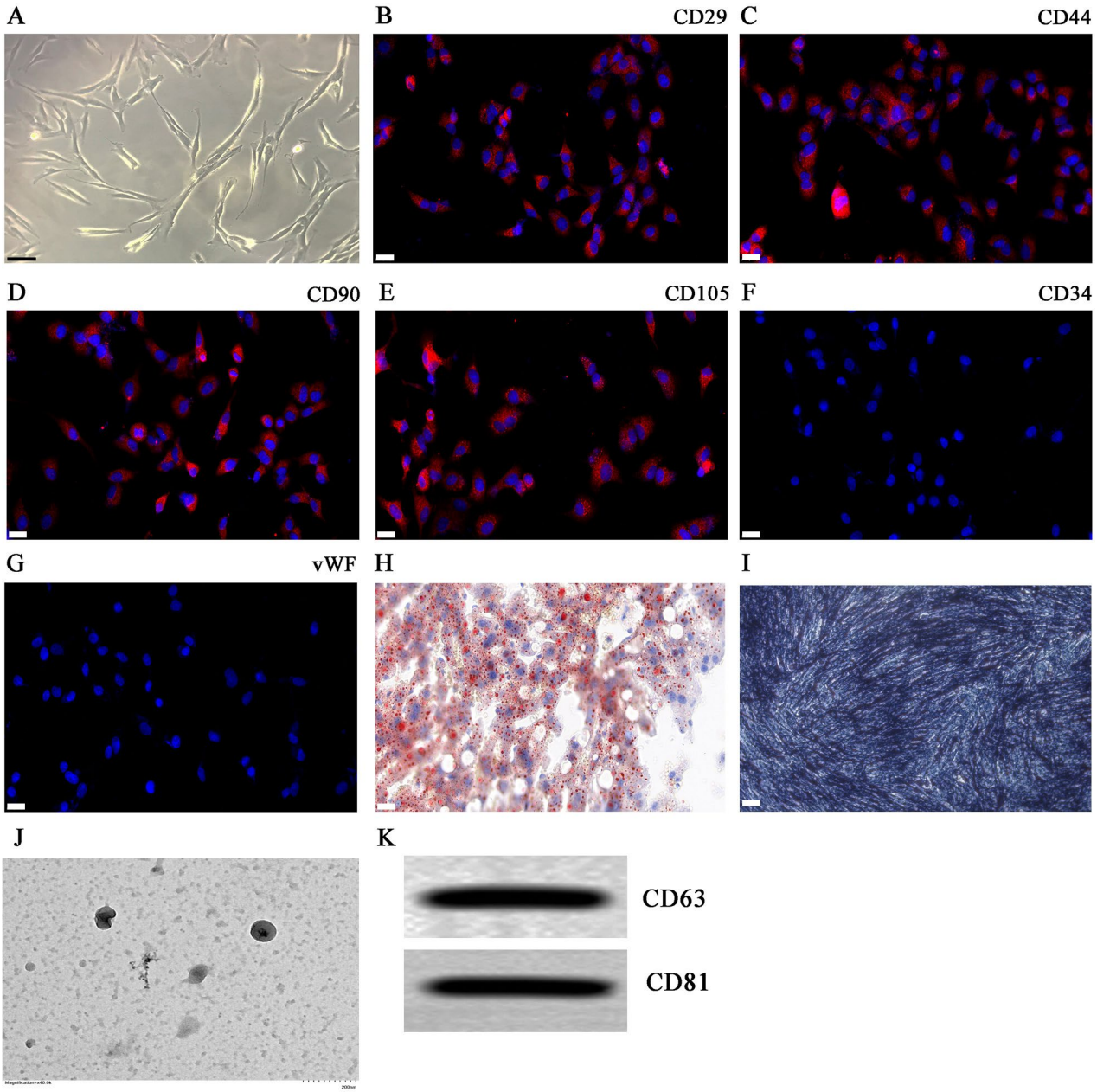

Fig. 1 Characterization of exosomes released by adipose-derived mesenchymal stem cells. **A** ADSCs showed a typical cobblestone-like morphology. Scale bar: 30 μm. **B–G** Immunofluorescence staining of cell surface markers. The antibodies were labeled with either fluorescein isothiocyanate (FITC, green) or phycoerythrin (PE, red). CD29, CD90, CD44, and CD105 are positive. CD34 and von Willebrand Factor (vWF) are negative. PE labeled mouse IgG isotype controls are shown. Differentiation potential of ADSCs assessed by oil red O (**H**) and alkaline phosphatase staining (**I**). **J** Transmission electron micrographs showing ADSC-exosome morphology. Scale bar: 150 nm. **K** Western blots of CD63 and CD81 expression in exosomes from ADSCs

wild-type (WT) cells, though not in mutated (MUT) cell lines (Fig. 4A, B), revealing that miR-15a-5p is circ-Stt3b target.

Bioinformatics data also suggested that GPX4 is a miR-15a-5p downstream target. To further verify correlations between GPX4 and miR-15a-5p, WT or MUT 3′UTR-GPX4 sequences, including miR-15a-5p binding sequence, were incorporated into a luciferase reporter vector (Fig. 4C). It was then transfected into HEK293 cells combined with or without the miR-15a-5p mimic. Luciferase reporter outcomes showed that miR-15a-5p suppressed the luciferase activity in WT cells, but not in MUT cell lines (Fig. 4D), demonstrating that GPX4 is an miR-15a-5p target.

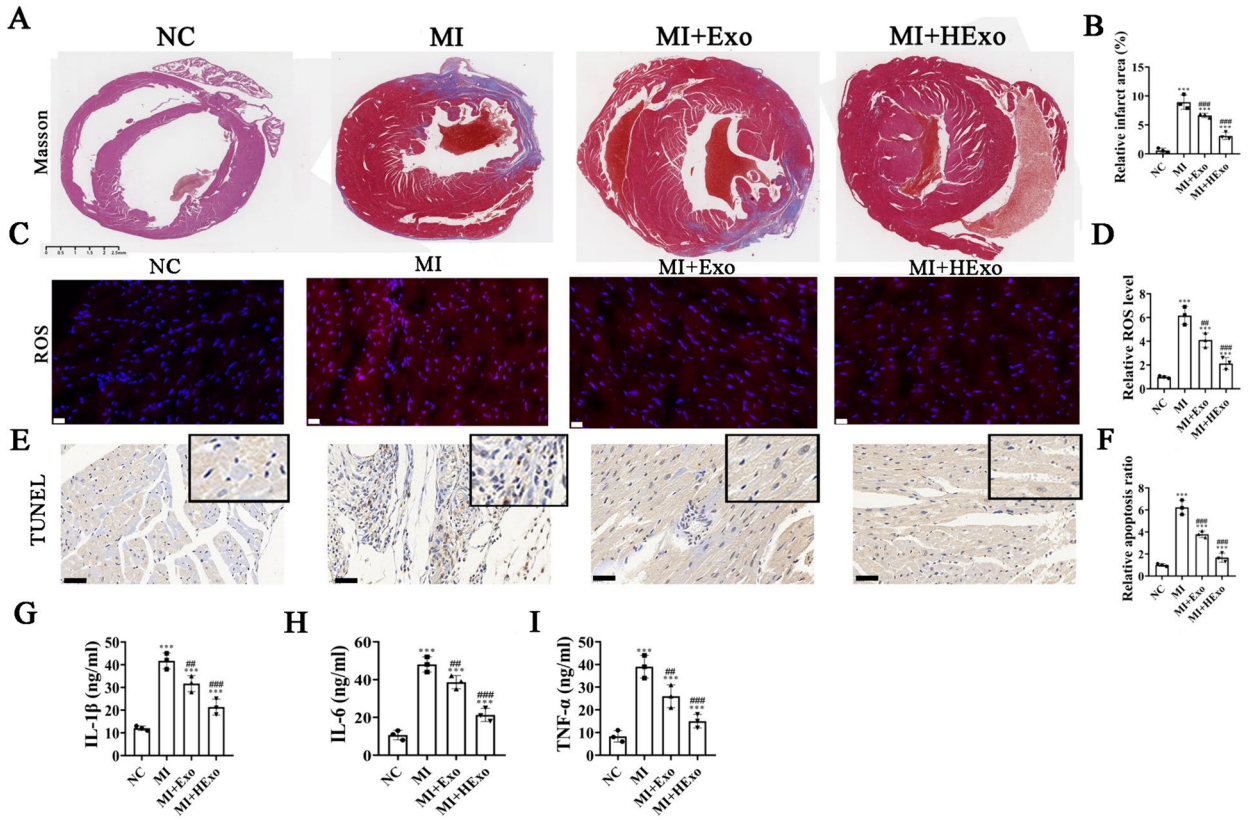

Fig. 2 Hypoxic pretreatment ADSCs exosome (HExo) have more treatment effect than ADSCs exosome (Exo) in ameliorate cardiac damage after myocardial infarction (MI). **A**, **B** The myocardial pathological morphology by masson staining. Data are means ± SD; ***$P < 0.001$ vs. NC. $^{\#\#\#}P < 0.001$ vs. MI. **C**, **D** Immunofluorescence for DCFH-DA staining show the ROS level. Data are means ± SD; ***$P < 0.001$ vs. NC. $^{\#\#\#}P < 0.001$ vs. MI. **E**, **F** Immunofluorescence for TUNEL staining show the apoptosis of myocardial tissue at the ischemic site. Data are means ± SD; ***$P < 0.001$ vs. NC. $^{\#\#\#}P < 0.001$ vs. MI. **G–I** ELISA detection show the inflammatory cytokines TNF-α, IL-6, and IL-1β expression in serum. Data are means ± SD; ***$P < 0.001$ vs. NC. $^{\#\#\#}P < 0.001$ vs. MI

qRT-PCR outcomes showed that circ-Stt3b expression incremented post-transfection with circ-Stt3b overexpression vector. The miR-15a-5p overexpression or GPX4 silencing did not affect circ-Stt3b expression in HL-1 cells (Fig. 4E), suggesting that both GPX4 and miR-15a-5p are the circ-Stt3b downstream targets. qRT-PCR outputs demonstrated that circ-Stt3b overexpression decreased miR-15a-5p expression. GPX4 silencing did not restored miR-15a-5p expression level after si-circ-Stt3b (Fig. 4F), advising that miR-15a-5p is located downstream of circ-Stt3b. The results also showed that GPX4 silencing decreased the GPX4 expression. However, miR-15a-5p upregulation reversed the promotion effects of circ-Stt3b to GPX4 expression. GPX4 expression was significantly decreased post-transfection with GPX4 silencing vector (Fig. 4G) saying that circ-Stt3b promoted GPX4 expression via sponging miR-15a-5p.

GPX4 Downregulation or miR-15a-5p Overexpression Reversed circ-Stt3b Protective Effects Upon HL-1 Cells After Exposure to Hypoxic Microenvironment

ELISA detection of inflammatory cytokine IL-6, IL-1β and TNF-α expressions showed that GPX4 downregulation or miR-15a-5p mimic (overexpression) reversed inhibitory effects regarding circ-Stt3b on inflammatory cytokine expression in HL-1 cells after exposure to a hypoxic microenvironment (Fig. 5A–C). HL-1 cell apoptosis evaluation results using flow cytometry showed that GPX4 downregulation or miR-15a-5p mimic (overexpression) reversed circ-Stt3b protective effect upon cell apoptosis after exposure to hypoxic conditions (Fig. 5D, E). ROS detection via immunofluorescence showed that

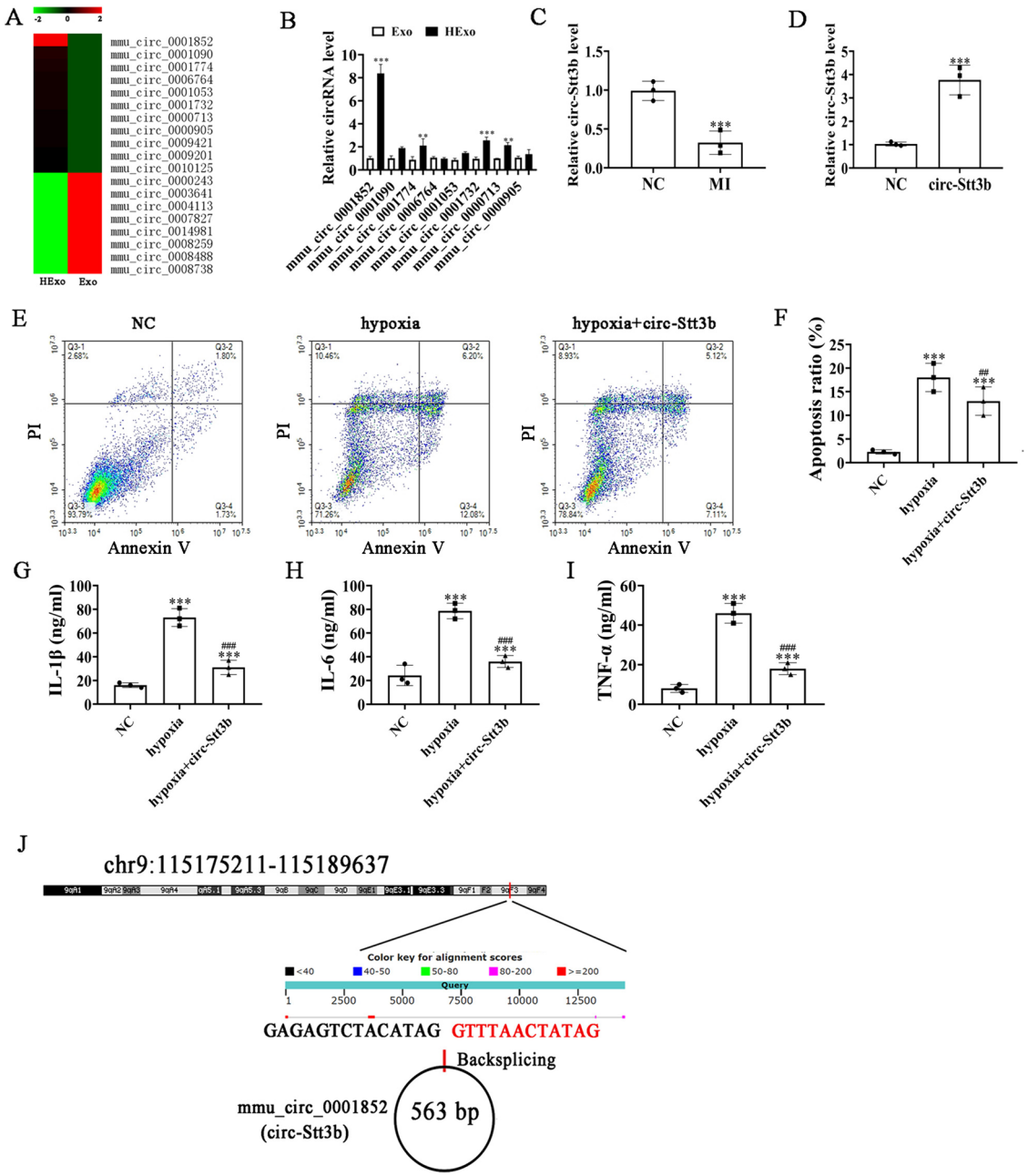

Fig. 3 Circ-Stt3b play a role in HExo-mediated cardiac damage repair after MI. **A** High-throughput sequencing analysis identified a series of upregulated and downregulated circRNAs between ADSCs exosome (Exo) and hypoxic pretreatment ADSCs exosome (HExo). **B** RT-qPCR detection show the expression of upregulation circRNA between Exo and HExo. Data are means ± SD; $^{**}P < 0.01$, $^{***}P < 0.001$ vs. Exo. **C** RT-qPCR detection show the expression of circ-Stt3b between NC and MI mice serum. Data are means ± SD; $^{***}P < 0.001$ vs. NC. **D** RT-qPCR detection show the expression of circ-Stt3b in HL-1 cells after transfected with circ-Stt3b overexpression vector (circ-Stt3b) or negative control vector (NC). Data are means ± SD; $^{***}P < 0.001$ vs. NC. **E**, **F** HL-1 cells apoptosis was assayed by flow cytometry after annexin V-FITC staining. Data are means ± SD; $^{***}P < 0.001$ vs. NC. $^{\#\#}P < 0.01$ vs. hypoxia. **G–I** ELISA detection show the inflammatory cytokines TNF-α, IL-6, and IL-1β expression. Data are means ± SD; $^{***}P < 0.001$ vs. NC. $^{\#\#\#}P < 0.001$ vs. hypoxia. **J** The genomic loci of the Stt3b gene and circ-Stt3b

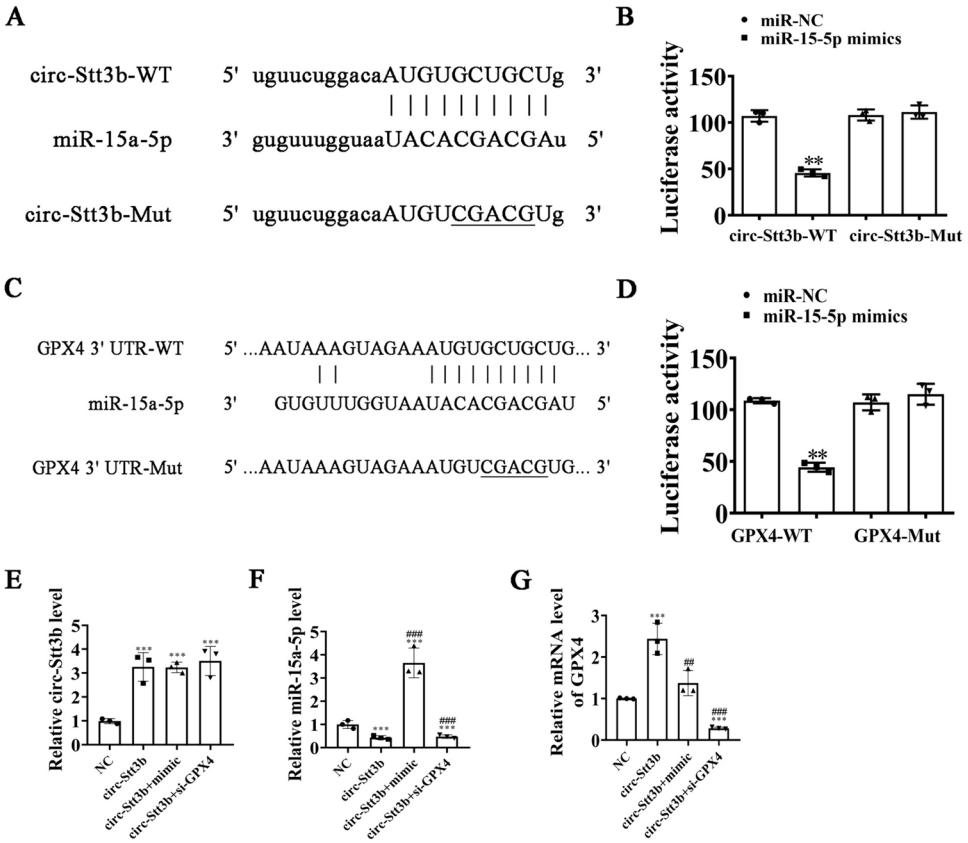

Fig. 4 MiR-15a-5p and GPX4 were downstream targets of circ-Stt3b. **A** Bioinformatics analysis predicting binding sites of miR-15a-5p in circ-Stt3b. Mutant version of circ-Stt3b is shown. **B** Relative luciferase activity determined 48 h after transfection of HEK293T cells with miR-15a-5p mimic/NC or circ-Stt3b wild-type/Mut. Data are means ± SD. $^{**}P < 0.01$. **C** Prediction of miR-15a-5p binding sites in the 3′-UTR of GPX4. Mutant version of 3′-UTR-GPX4 is shown. **D** Relative luciferase activity 48 h after transfection of HEK293T cells with miR-15a-5p mimic/NC or 3′-UTR-GPX4 wild-type/Mut. Data are means ± SD. $^{**}P < 0.01$. RT-qPCR showing expression of circ-Stt3b (**E**), miR-15a-5p (**F**), GPX4 (**G**) in HL-1 cells. Data are means ± SD. $^{***}P < 0.001$ vs. NC. $^{\#\#}P < 0.01$, $^{\#\#\#}P < 0.001$ vs. circ-Stt3b

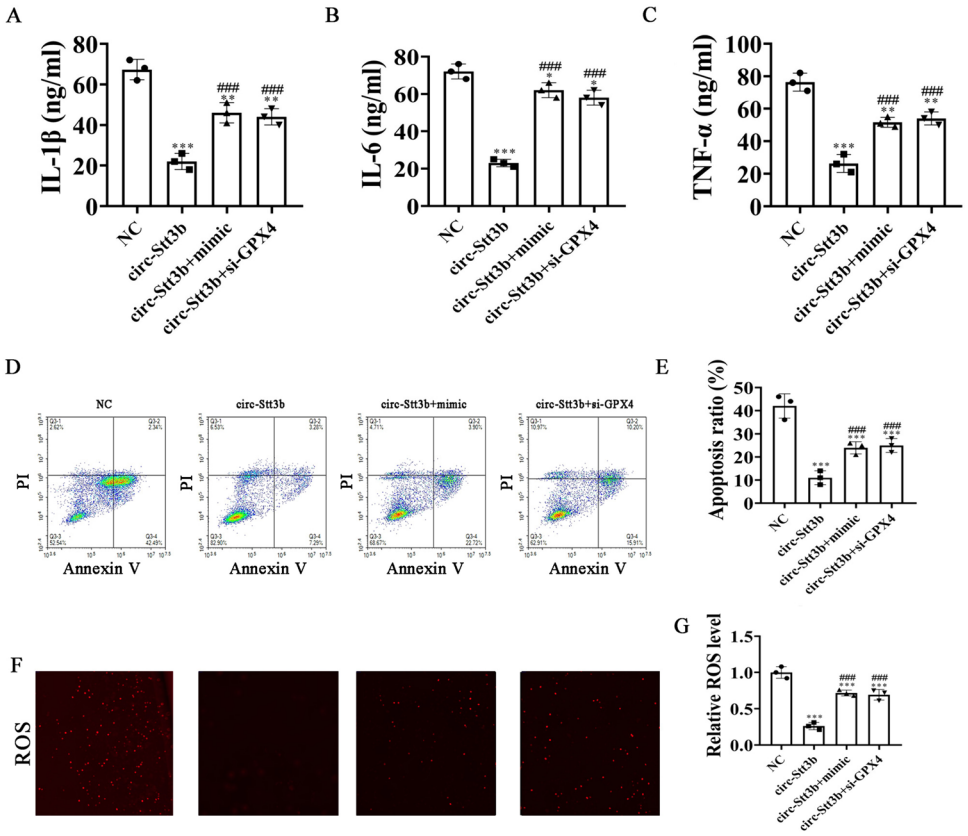

Fig. 5 Downregulation of GPX4 or overexpression of miR-15a-5p reversed the protective effect of circ-Stt3b to HL-1 after exposure to hypoxia microenvironment. **A**–**C** ELISA detection show the inflammatory cytokines TNF-α, IL-6, and IL-1β expression. Data are means ± SD; $^{*}P < 0.05$, $^{**}P < 0.01$, $^{***}P < 0.001$ vs. NC. $^{\#\#\#}P < 0.001$ vs. circ-Stt3b. **D**, **E** HL-1 cells apoptosis was assayed by flow cytometry after annexin V-FITC staining. Data are means ± SD; $^{***}P < 0.001$ vs. NC. $^{\#\#\#}P < 0.001$ vs. circ-Stt3b. **F**, **G** Immunofluorescence for DCFH-DA staining show the ROS level. Data are means ± SD; $^{***}P < 0.001$ vs. NC. $^{\#\#\#}P < 0.001$ vs. circ-Stt3b

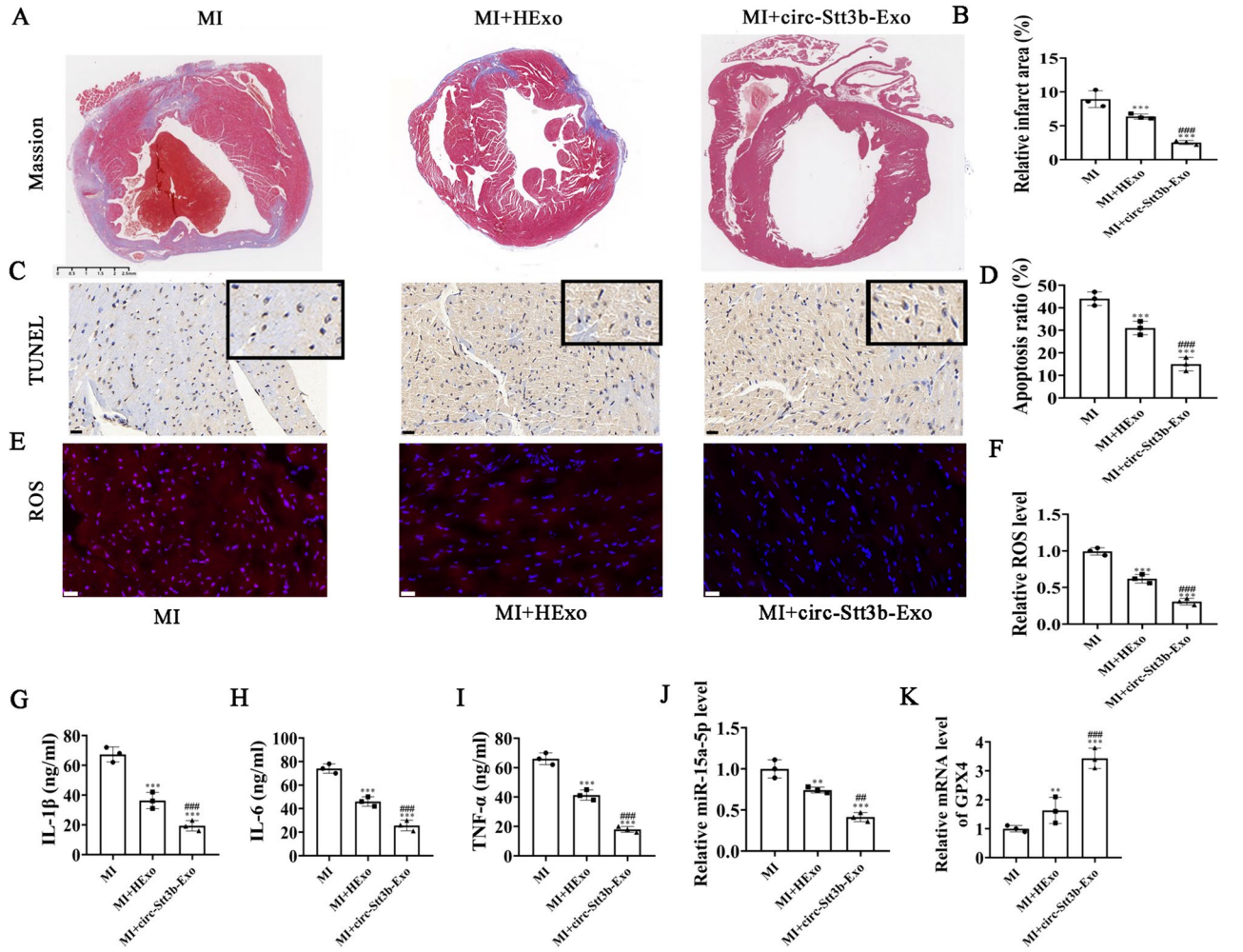

Fig. 6 Overexpression circ-Stt3b increased treatment effect of ADSCs Exo in ameliorate cardiac damage after MI. **A**, **B** The myocardial pathological morphology by masson staining. Data are means ± SD; ***$P < 0.001$ vs. MI. $^{###}P < 0.001$ vs. MI + HExo. **C**, **D** Immunofluorescence for DCFH-DA staining show the ROS level. Data are means ± SD; ***$P < 0.001$ vs. MI. $^{###}P < 0.001$ vs. MI + HExo. **E**, **F** Immunofluorescence for TUNEL staining show the apoptosis of myocardial tissue at the ischemic site. Data are means ± SD; ***$P < 0.001$ vs. MI. $^{###}P < 0.001$ vs. MI + HExo. **G**–**I** ELISA detection show the inflammatory cytokines TNF-α, IL-6, and IL-1β expression in serum. Data are means ± SD; ***$P < 0.001$ vs. MI. $^{###}P < 0.001$ vs. MI + HExo. **J**, **K** RT-qPCR detection show the expression of miR-15a-5p and GPX4. Data are means ± SD; ***$P < 0.001$ vs. MI. $^{###}P < 0.001$ vs. MI + HExo

GPX4 downregulation or miR-15a-5p overexpression reversed inhibitory effect of circ-Stt3b upon hypoxia-induced ROS (Fig. 5F, G).

circ-Stt3b Overexpression Increased the ASDSC Exo Treatment Effect of Ameliorating Cardiac Damage After MI

Masson's trichrome staining to detect the infarcted tissue size after 28 days identified the fibrotic areas in blue. The results showed that Exos from circ-Stt3b overexpression ADSCs (circ-Stt3b-Exo) held greater therapeutic effects by reducing the MI-induced myocardial damage compared to HExos (Fig. 6A, B). Immunofluorescence ROS analysis showed that circ-Stt3b-Exos had a greater therapeutic effect by decreasing MI-induced myocardial ROS levels in the infarction area (Fig. 6C, D). TUNEL staining showcased that circ-Stt3b-Exo held greater therapeutic effects by reducing MI-induced myocardial apoptosis (Fig. 6E, F). ELISA data validated that circ-Stt3b-Exo had greater therapeutic effects than HExos by reducing MI-induced inflammatory cytokine IL-6, IL-1β and TNF-α expression levels in serum (Fig. 6G–I). The RT-qPCR data showcased that circ-Stt3b-Exo treatment held greater effects by decreasing miR-15a-5p (Fig. 6J) and increasing GPX4 expression than HExos (Fig. 6K).

Discussion

The present investigation successfully isolated ADSCs and ADSC exosomes. Exosomes from ADSCs and especially those with hypoxic pretreatment had a greater therapeutic effect on cardiac damage amelioration post-MI. Accumulation studies verified that circRNAs have an indispensable function in microenvironmental regulations [21]. CircRNA delivery was utilized to define if ADSC exosomes influence MI-induced myocardial damage. NGS analysis identified the abnormally expressed circRNAs among Exos and HExos. Data showcased that circ-Stt3b levels increased within the exosomes from hypoxic pretreatment ADSCs. The circ-Stt3b downregulation decreased the therapeutic effect of HExos on MI-induced myocardial damage, including apoptosis, ROS level, and inflammatory factor expression. The circ-Stt3b overexpression decreased the hypoxia-induced myocardial cell apoptosis, ROS level, and inflammatory factor expression, suggesting that circ-Stt3b plays a role in HExo-mediated cardiac damage repair after MI.

Bioinformatics and luciferase report analysis of circ-Stt3b showed that it can interact with miR-15a-5p. Furthermore, circ-Stt3b overexpression decreased miR-15a-5p expression. Prior research has shown that miR-15a-5p was upregulated after MI [22]. The miR-15a-5p inhibitor significantly inhibited inflammatory factor secretion [23]. Current investigations also illustrated that miR-15a-5p downregulation decreased stress-induced cell apoptosis [24]. Downregulating miR-15a-5p decreased the ROS production [25]. The current investigation also found that miR-15a-5p overexpression reversed protective effect regarding circ-Stt3b upon HL-1 cells after exposure to a hypoxic microenvironment.

Further investigation using bioinformatics and luciferase reporter data showed that GPX4 is a miR-15a-5p downstream target. In addition, circ-Stt3b overexpression promoted GPX4 expression. Previous studies have found that glutathione peroxidase 4 (GPX4) was downregulated in early and middle MI stages, which protects cells from ferroptosis [25]. The study also found that GPX4 downregulation reversed protective effect regarding circ-Stt3b upon HL-1 cells post exposing to hypoxic conditions. Overexpression of circ-Stt3b incremented treatment effect of ADSC Exos on ameliorating cardiac damage after MI by decreasing the level of ROS, inflammatory factors, and myocardial apoptosis. This suggests that circ-Stt3b expression promotes GPX4 by sponging miR-15a-5p. The upregulated GPX4 expression decreased the level of MI-induced ROS and ferroptosis.

Conclusion

In summary, our study determined that exosomes from hypoxic pretreatment ADSCs ameliorate cardiac damage after MI through activation of circ-Stt3b/miR-15a-5p/GPX4 signaling and decreased ferroptosis. With the wide interest in exosome from both academia and the pharmaceutical industry, there is no doubt that clinical application will continually evolve and improve, which will help to advance exosome studies in cardiovascular science.

Supplementary Information The online version contains supplementary material available at https://doi.org/10.1007/s12012-024-09915-9.

Acknowledgements None.

Author Contributions JL, ZW, and AL performed research and analyzed results. JL, ZW, and AL discussed results. NZ edited the paper, designed the research and drafted the paper. JL, ZW, and AL conceived the study. All authors approved the final manuscript.

Funding None.

Data Availability The datasets used and/or analyzed during the current study are available from the corresponding author on reasonable request.

Declarations

Conflict of interest All the authors declare that they have no conflict of interest.

Ethical Approval The animal studies were performed after receiving approval of the Institutional Animal Care and Use Committee in Shanxi Hospital of Traditional Chinese Medicine.

Consent for Publication Not applicable.

References

1. BayesdeLuna, A., & Guindo, J. (1990). Sudden death in ischemic heart disease. *Revista Portuguesa de Cardiologia, 9*, 473–479.
2. Li, W., Leng, Y., Xiong, Y., & Xia, Z. (2020). Ferroptosis is involved in diabetes myocardial ischemia/reperfusion injury

through endoplasmic reticulum stress. *DNA and Cell Biology, 39*, 210–225.
3. Stockwell, B. R., Jiang, X., & Gu, W. (2020). Emerging mechanisms and disease relevance of ferroptosis. *Trends in Cell Biology, 30*, 478–490.
4. Ma, S., Sun, L., Wu, W., Wu, J., Sun, Z., & Ren, J. (2020). USP22 protects against myocardial ischemia-reperfusion injury via the SIRT1-p53/SLC7A11-dependent inhibition of ferroptosis-induced cardiomyocyte death. *Frontiers in Physiology, 11*, 551318.
5. Li, T., Tan, Y., Ouyang, S., He, J., & Liu, L. (2022). Resveratrol protects against myocardial ischemia-reperfusion injury via attenuating ferroptosis. *Gene, 808*, 145968.
6. Shan, X., Lv, Z. Y., Yin, M. J., Chen, J., Wang, J., & Wu, Q. N. (2021). The protective effect of cyanidin-3-glucoside on myocardial ischemia-reperfusion injury through ferroptosis. *Oxidative Medicine and Cellular Longevity, 2021*, 8880141.
7. Song, Y., Wang, B., Zhu, X., Hu, J., Sun, J., Xuan, J., & Ge, Z. (2021). Human umbilical cord blood-derived mscs exosome attenuate myocardial injury by inhibiting ferroptosis in acute myocardial infarction mice. *Cell Biology and Toxicology, 37*, 51–64.
8. Zhu, L. P., Tian, T., Wang, J. Y., He, J. N., Chen, T., Pan, M., Xu, L., Zhang, H. X., Qiu, X. T., Li, C. C., Wang, K. K., Shen, H., Zhang, G. G., & Bai, Y. P. (2018). Hypoxia-elicited mesenchymal stem cell-derived exosomes facilitates cardiac repair through miR-125b-mediated prevention of cell death in myocardial infarction. *Theranostics, 8*, 6163–6177.
9. Zhang, L., Li, K., Liu, X., Li, D., Luo, C., Fu, B., Cui, S., Zhu, F., Zhao, R. C., & Chen, X. (2013). Repeated systemic administration of human adipose-derived stem cells attenuates overt diabetic nephropathy in rats. *Stem Cells and Development, 22*, 3074–3086.
10. Gao, W., Wang, X., Si, Y., Pang, J., Liu, H., Li, S., Ding, Q., & Wang, Y. (2021). Exosome derived from ADSCs attenuates ultraviolet B-mediated photoaging in human dermal fibroblasts. *Photochemistry and Photobiology, 97*, 795–804.
11. Deng, S., Zhou, X., Ge, Z., Song, Y., Wang, H., Liu, X., & Zhang, D. (2019). Exosomes from adipose-derived mesenchymal stem cells ameliorate cardiac damage after myocardial infarction by activating S1P/SK1/S1PR1 signaling and promoting macrophage M2 polarization. *International Journal of Biochemistry & Cell Biology, 114*, 105564.
12. Liu, Z., Xu, Y., Wan, Y., Gao, J., Chu, Y., & Li, J. (2019). Exosomes from adipose-derived mesenchymal stem cells prevent cardiomyocyte apoptosis induced by oxidative stress. *Cell Death Discovery, 5*, 79.
13. Pegtel, D. M., & Gould, S. J. (2019). Exosomes. *Annual Review of Biochemistry, 88*, 487–514.
14. Kalluri, R., & LeBleu, V. S. (2020). The biology, function, and biomedical applications of exosomes. *Science, 367*, eaau6977.
15. Kristensen, L. S., Andersen, M. S., Stagsted, L. V. W., Ebbesen, K. K., Hansen, T. B., & Kjems, J. (2019). The biogenesis, biology and characterization of circular RNAs. *Nature Reviews Genetics, 20*, 675–691.
16. Garikipati, V. N. S., Verma, S. K., Cheng, Z., Liang, D., Truongcao, M. M., Cimini, M., Yue, Y., Huang, G., Wang, C., Benedict, C., Tang, Y., Mallaredy, V., Ibetti, J., Grisanti, L., Schumacher, S. M., Gao, E., Rajan, S., Wilusz, J. E., Goukassian, D., …, Kishore, R. (2019). Circular RNA CircFndc3b modulates cardiac repair after myocardial infarction via FUS/VEGF-A axis. *Nature Communications, 10*, 4317.
17. Bai, M., Pan, C. L., Jiang, G. X., & Zhang, Y. M. (2020). CircRNA 010567 improves myocardial infarction rats through inhibiting TGF-beta1. *European Review for Medical and Pharmacological Sciences, 24*, 369–375.
18. Hu, N., Cai, Z., Jiang, X., Wang, C., Tang, T., Xu, T., Chen, H., Li, X., Du, X., & Cui, W. (2023). Hypoxia-pretreated ADSC-derived exosome-embedded hydrogels promote angiogenesis and accelerate diabetic wound healing. *Acta Biomaterialia, 157*, 175–186.
19. Jin, J., Shi, Y., Gong, J., Zhao, L., Li, Y., He, Q., & Huang, H. (2019). Exosome secreted from adipose-derived stem cells attenuates diabetic nephropathy by promoting autophagy flux and inhibiting apoptosis in podocyte. *Stem Cell Research & Therapy, 10*, 95.
20. Shi, R., Jin, Y., Hu, W., Lian, W., Cao, C., Han, S., Zhao, S., Yuan, H., Yang, X., Shi, J., & Zhao, H. (2020). Exosomes derived from mmu_circ_0000250-modified adipose-derived mesenchymal stem cells promote wound healing in diabetic mice by inducing miR-128-3p/SIRT1-mediated autophagy. *American Journal of Physiology. Cell Physiology, 318*, C848–C856.
21. Zhang, M., Wang, Z., Cheng, Q., Lv, X., & Li, N. (2020). Circular RNA (circRNA) CDYL induces myocardial regeneration by cerna after myocardial infarction. *Medical Science Monitor, 26*, e923188.
22. Fan, K., Huang, W., Qi, H., Song, C., He, C., Liu, Y., Zhang, Q., Wang, L., & Sun, H. (2021). The Egr-1/miR-15a-5p/GPX4 axis regulates ferroptosis in acute myocardial infarction. *European Journal of Pharmacology, 909*, 174403.
23. Lou, Y., & Huang, Z. (2020). microRNA-15a-5p participates in sepsis by regulating the inflammatory response of macrophages and targeting TNIP2. *Experimental and Therapeutic Medicine, 19*, 3060–3068.
24. Hong, X., Li, S., Wang, J., Zhao, Z., & Feng, Z. (2021). Circular RNA circFADS2 is overexpressed in sepsis and suppresses LPS-induced lung cell apoptosis by inhibiting the maturation of miR-15a-5p. *BMC Immunology, 22*, 29.
25. Yao, B., Ye, L., Chen, J., Zhuo, S., & Lin, H. (2021). Linc00473 protects against cerebral ischemia reperfusion injury via sponging miR-15b-5p and miR-15a-5p to regulate SRPK1 expression. *Brain Injury, 35*, 1462–1471.